Electronic Supplementary Material (ESI) for Physical Chemistry Chemical Physics.

Supporting Materials Section for

Proton-phosphorous connectivities revealed by high-resolution proton-detected solid-state NMR

Alexander A. Malär[a], Qiu Sun[b], Johannes Zehnder[a], Gerald Kehr[b], Gerhard Erker[b], and Thomas Wiegand[a,c,d,*]

[a]*Physical Chemistry, ETH Zurich, Vladimir-Prelog-Weg 2, 8093 Zurich, Switzerland*

[b] *Organisch-Chemisches Institut, WWU Münster, Corrensstr. 40, 48149 Münster, Germany*

[c] *Max-Planck-Institute for Chemical Energy Conversion, Stiftstr. 34-36, 45470 Mülheim an der Ruhr, Germany (new address)*

[d] *Institute of Technical and Macromolecular Chemistry, RWTH Aachen University, Worringerweg 2, 52074 Aachen, Germany (new address)*

[*]Corresponding author: thomas.wiegand@cec.mpg.de

Supplementary Figures

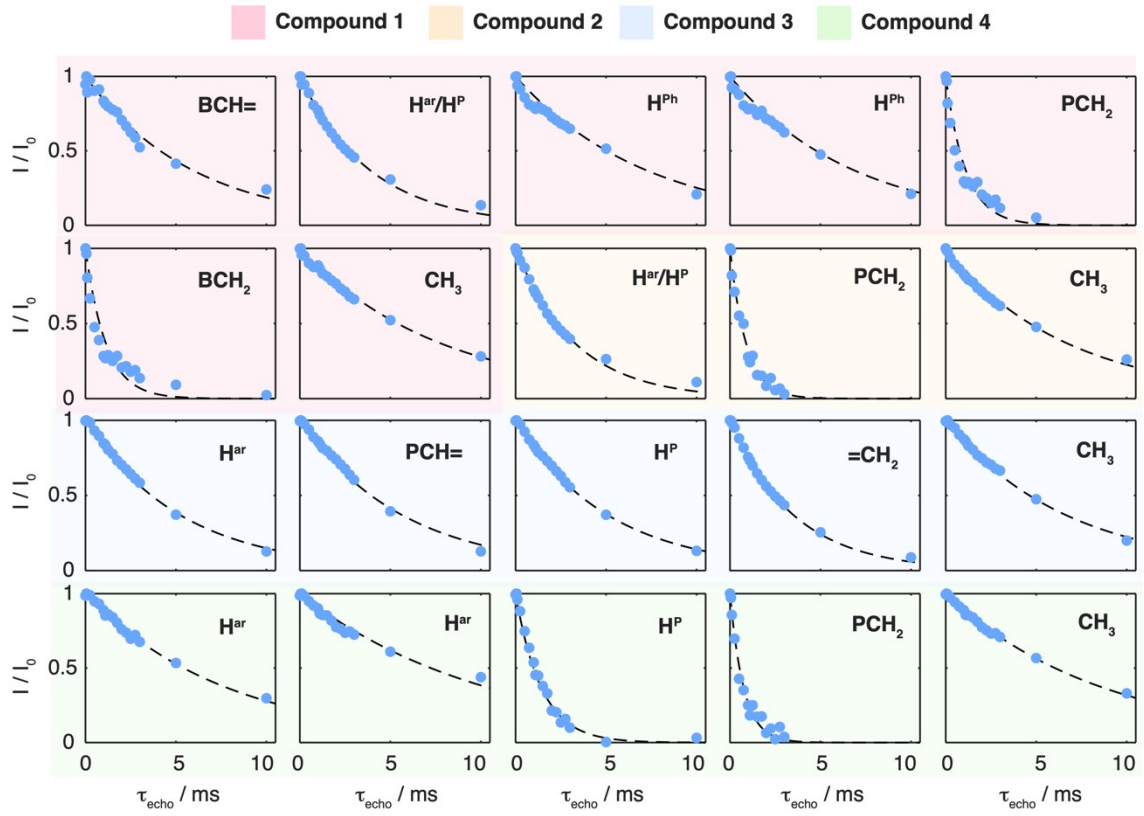

Figure S1: T_2'(^{1}H) relaxation decay curves for compounds **1-4**, using Hahn-echo relaxation experiments with variable echo time τ_{echo}. Dashed lines denote the corresponding mono-exponential fits of the raw data using the functional form ($A \cdot \exp(-\tau_{echo}/B)$).

	δ_{iso}/ ppm	Δ^{total}/Hz	Δ^{homo}/Hz	Δ^{inhomo}/Hz
BCH=	8.2	376	53	323
H^{Ph}	5.3	289	44	245
H^{Ph}	4.1	286	46	240
PCH_2	3.4	320	287	33

Table S1: Summary of site-specific total (Δ^{total}), homogeneous (Δ^{homo}) and inhomogeneous (Δ^{inhomo}) proton linewidths in compound **1** at 100 kHz MAS and 20.0 T. Total linewidths have been obtained by fitting the ^{1}H-MAS spectrum with the software dmfit[1].

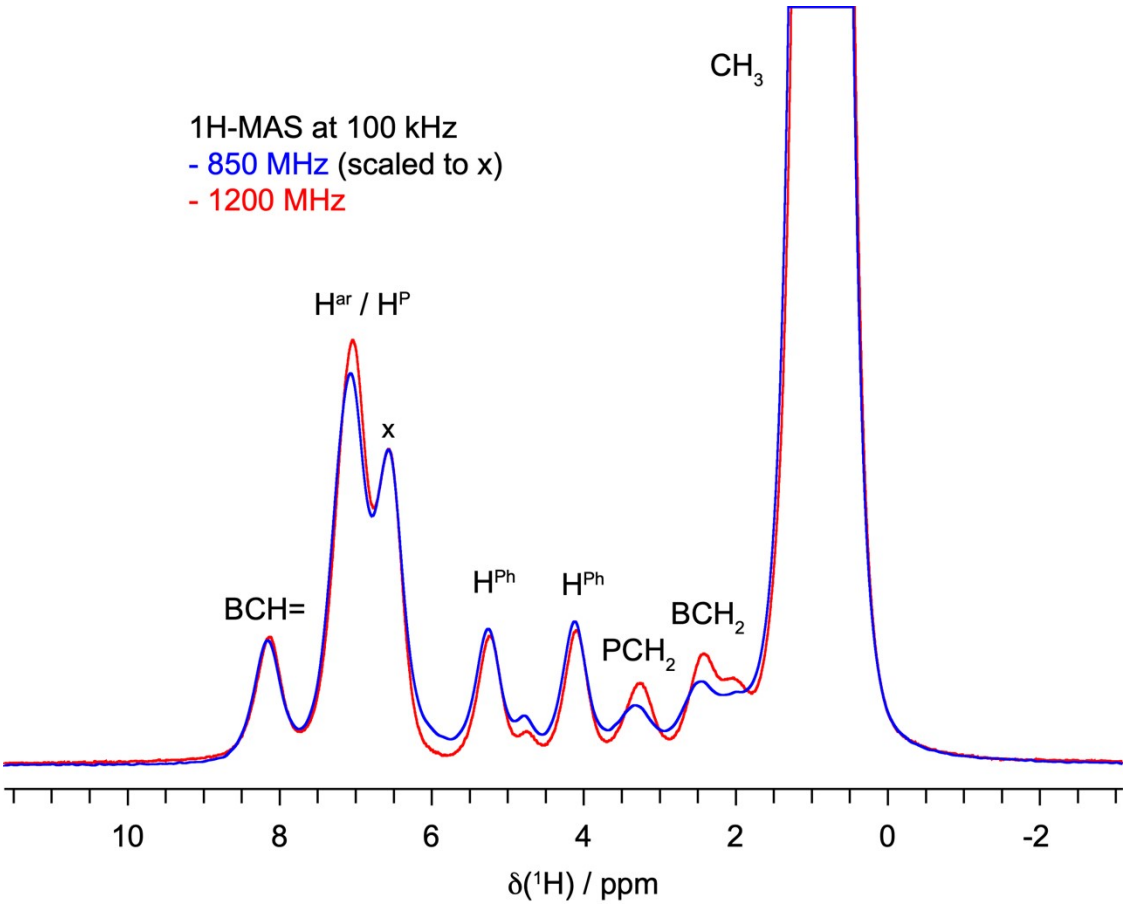

Figure S2: *Experiments at 1200 MHz on compound **1** indicate that homogenously broadened resonances (PCH_2, BCH_2) profit the most from the field increase, while the remaining resonances are mainly dominated by inhomogeneous broadening effects.* ^{1}H-detected MAS spectra recorded with a MAS frequency of 100 kHz at 20.0 T (blue) and 28.2 T (red).

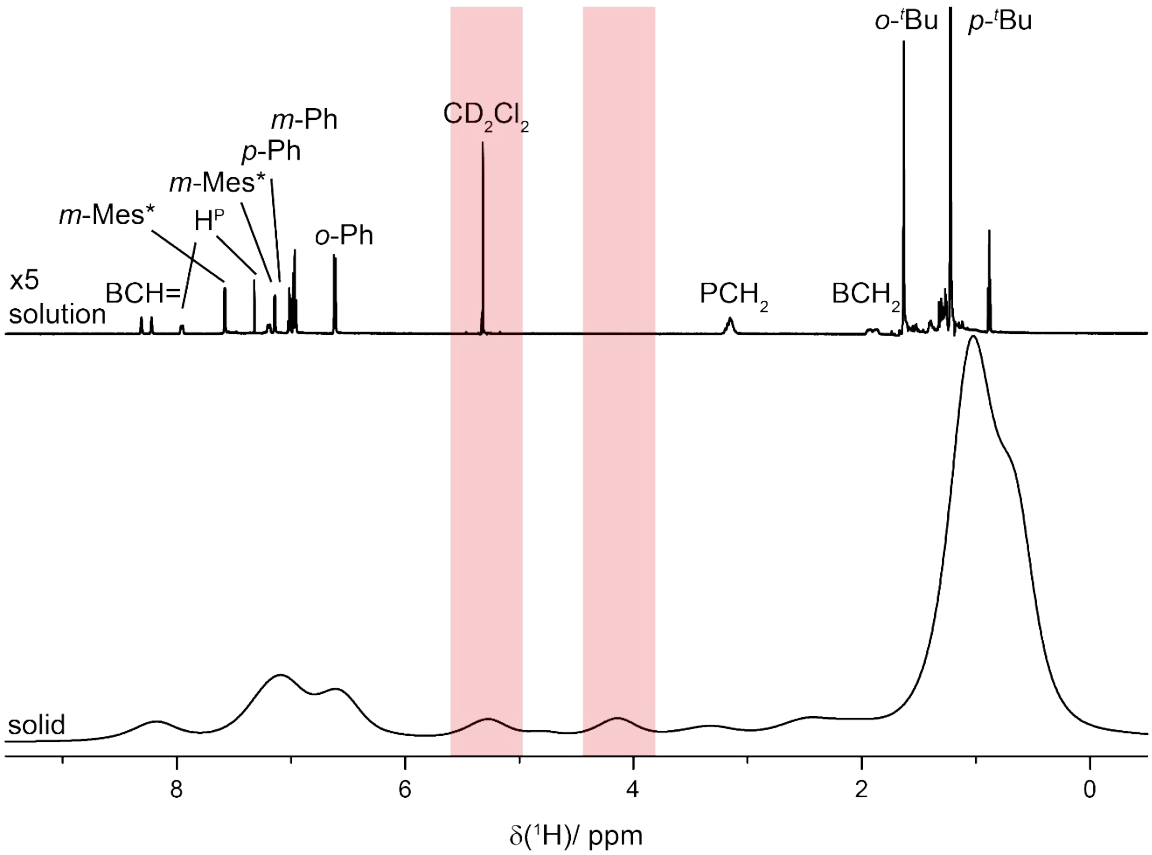

Figure S3: *Proton chemical-shift differences between solution and solid state.* Comparison of ^{1}H-detected solution- and solid-state NMR spectra of compound **1** recorded at 14.1 T (solvent CD_2Cl_2, taken from reference [2]) and 20.0 T with a MAS frequency of 100 kHz, respectively. The resonances highlighted in red are shifting to lower frequencies due to intermolecular ring current effects.

Section S1: Ring-current effect calculated by the Johnson-Bovey equation

The Johnson-Bovey equation in e.s.u. units is given as

$$\delta_R \, x \, 10^{-6} = \frac{-ne^2}{6\pi mc^2 a} \cdot \frac{1}{\left((1+\rho)^2 + z^2\right)^{0.5}} \cdot \left[K + \left(\frac{1-\rho^2-z^2}{(1-\rho)^2+z^2}\right) \cdot E\right] \quad (1)$$

where n is the number of π-electrons, a is the ring radius of 1.39 Å, e, m and c are the standard constants, K and E are the first and second complete elliptic integrals, which are a function of the geometric parameters ρ and z (Figure S4). ρ and z are given in units of a.

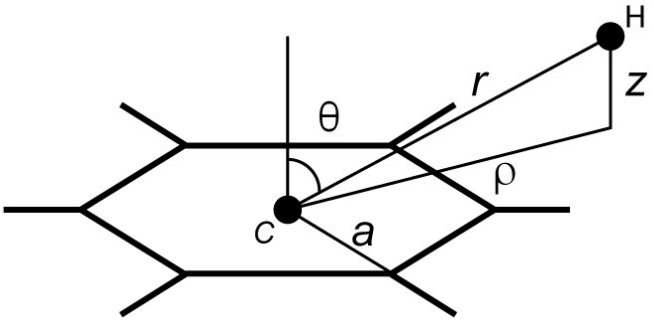

Figure S4: Definition of the geometric parameters used in the Johnson-Bovey equation.

The first and second complete elliptic integrals are

$$K(k) = \int_0^{\pi/2} \frac{1}{\sqrt{1-k^2 sin^2(\theta)^2}} \, d\theta \quad (2)$$

$$E(k) = \int_0^{\pi/2} \sqrt{1-k^2 sin^2(\theta)^2} \, d\theta \quad (3)$$

where θ is the angle between the vector joining the observed proton to the ring center (***r***) and the line perpendicular to the ring plane passing through the ring center *C* (Figure S3) and k is the modulus of the complete elliptic integrals expressed as

$$k = \left[\frac{4\rho}{(1+\rho)^2 + z^2}\right]^{0.5}. \quad (4)$$

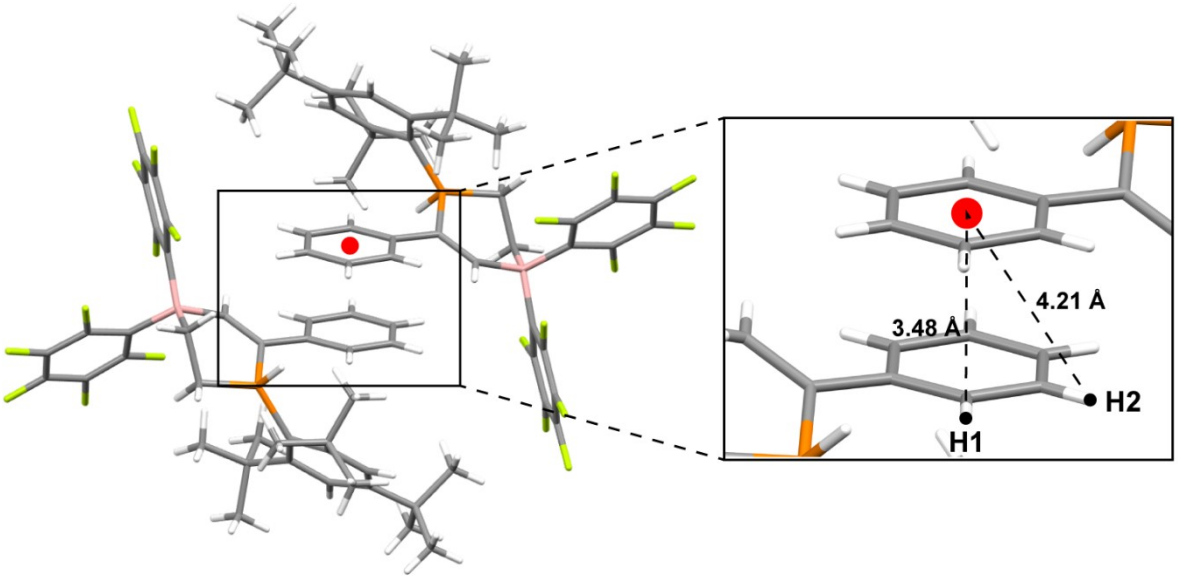

Figure S5: Intermolecular ring-current effects explaining the unusual chemical shifts of some phenyl protons in the solid state compared to liquid-state NMR of compound **1**. Intermolecular distances between the phenyl ring protons of one molecule and the centroid position (red sphere) of the partner phenyl ring are shown as black dashed lines.

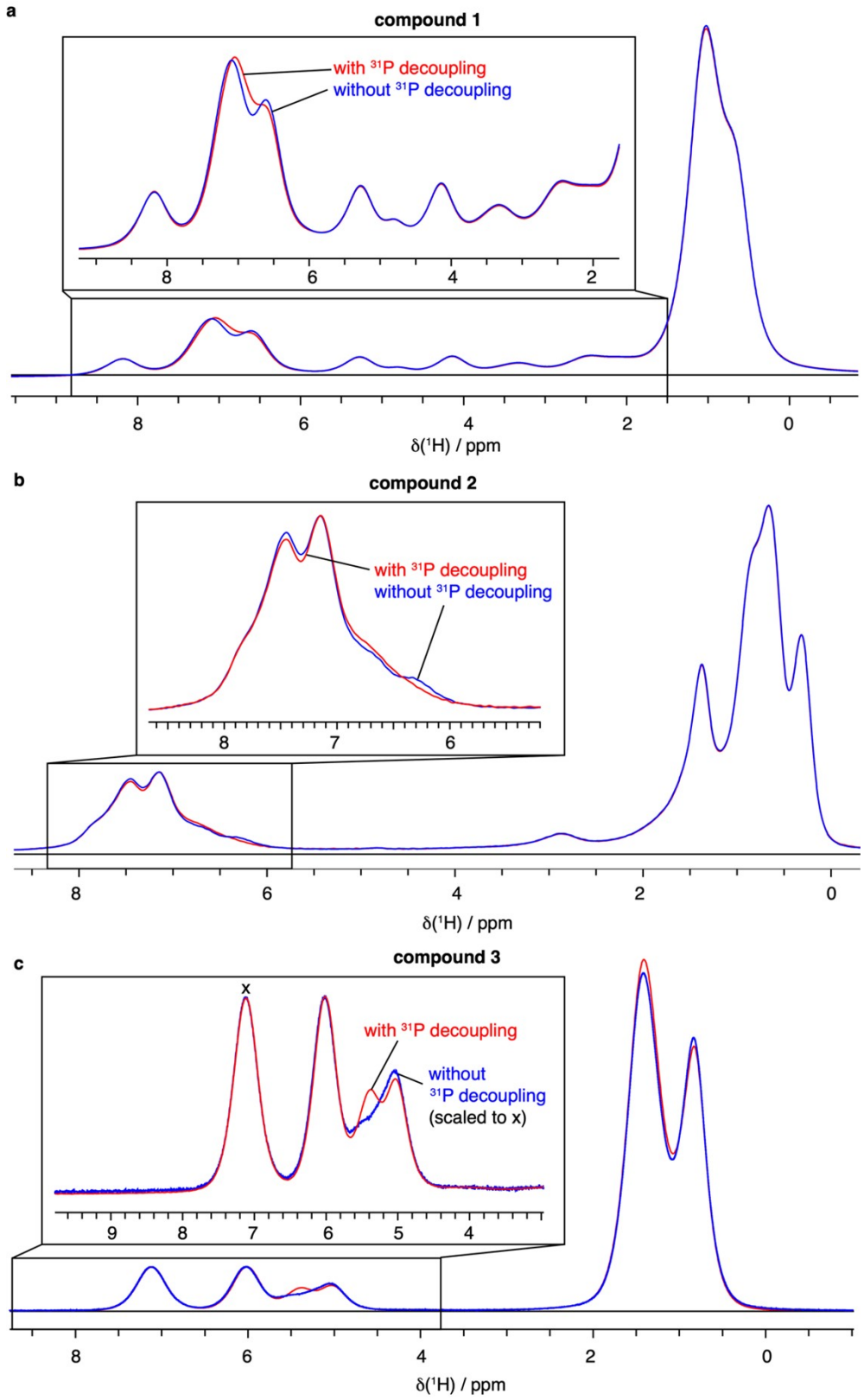

Figure S6: ^{1}H MAS spectra of **1 a, 2 b, 3 c**, recorded at 100 kHz and 20.0 T without ^{31}P decoupling during acquisition (blue spectrum) and with ^{31}P decoupling (red spectrum).

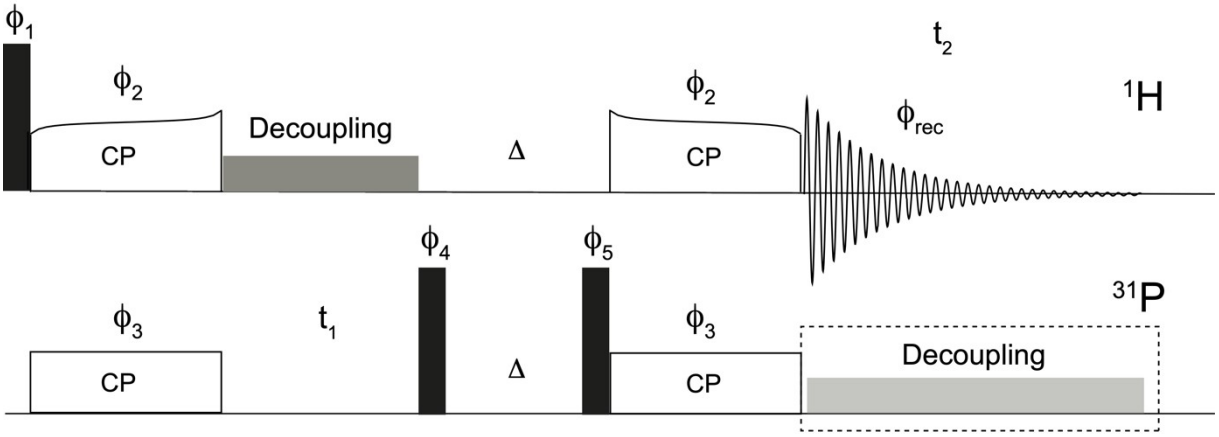

Figure S7: CP-hPH pulse sequence used for filtering ^{1}H-^{31}P connectivities. The pulse phase values are given as follows: $\phi_1 =$ *x x -x -x y y -y -y*, $\phi_2 =$ *y y y y -x -x -x -x*, $\phi_3 =$ *x x -x -x y y -y -y*, $\phi_4 =$ *-y -y y y x x -x -x*, $\phi_5 =$ *y -y -y y -x x x -x*, $\phi_{rec} =$ *x -x -x x y -y -y y*. Black squares denote 90° hard pulses, adiabatic shapes[3, 4] are applied during CP transfers. The sequence of 90° hard pulses on ^{31}P have been used for power level optimization and as a z-filter. Δ has been set to 5 ms. Low power ^{31}P decoupling during direct detection can be applied to quench resonance splitting induced by the ^{31}P *J* coupling.

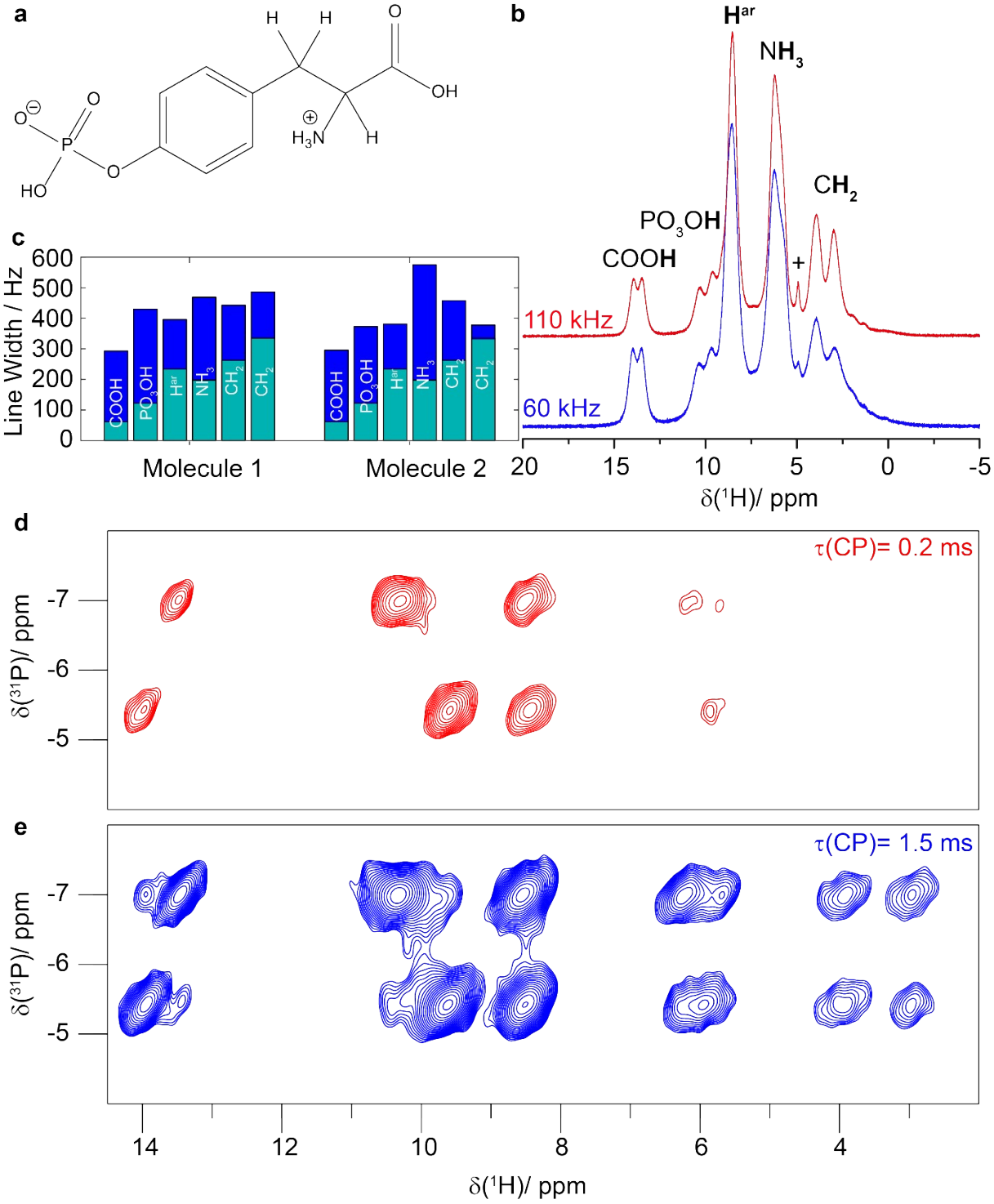

Figure S8: *Proton-phosphorus spatial proximities probed in ortho-phospho-L-tyrosine.* **a** Chemical structure. **b** ^{1}H MAS spectra recorded at a spinning frequency of 60 kHz (blue) and 110 kHz. **c** Homogeneous (cyan) and heterogeneous (blue) proton linewidths determined at a MAS frequency of 105 kHz for the two molecules in the asymmetric unit. hPH correlation spectra recorded with a proton-phosphorus (and vice versa) CP contact time of 0.2 ms (**d**) and 1.5 ms (**e**). The total ^{1}H line widths were determined using the 2D spectrum in **e** and the ccpnmr software[5-7].

Section S2: ^{1}H-detected solid-state NMR spectra of ortho-phospho-L-tyrosine

Figure S8 summarizes the ^{1}H MAS spectra and the proton line broadening contributions measured at 100 kHz MAS of ortho-phospho-L-tyrosine. In agreement with previous data, some proton resonances, comprising the phosphate -PO_3OH proton resonance, split into two lines possibly as a consequence of two molecules in the asymmetric unit as observed crystallographically[8]. The corresponding hPH spectra with different CP contact times are also given in Figure S8 and allow for the identification of the set of resonances belonging to one molecule by benefitting from the different ^{31}P shifts. The hPH spectrum at longer CP contact times (1 ms) indeed confirms that the two molecules are in spatial proximity due to weak cross-peaks between the ^{31}P and ^{1}H resonances of the different molecules.

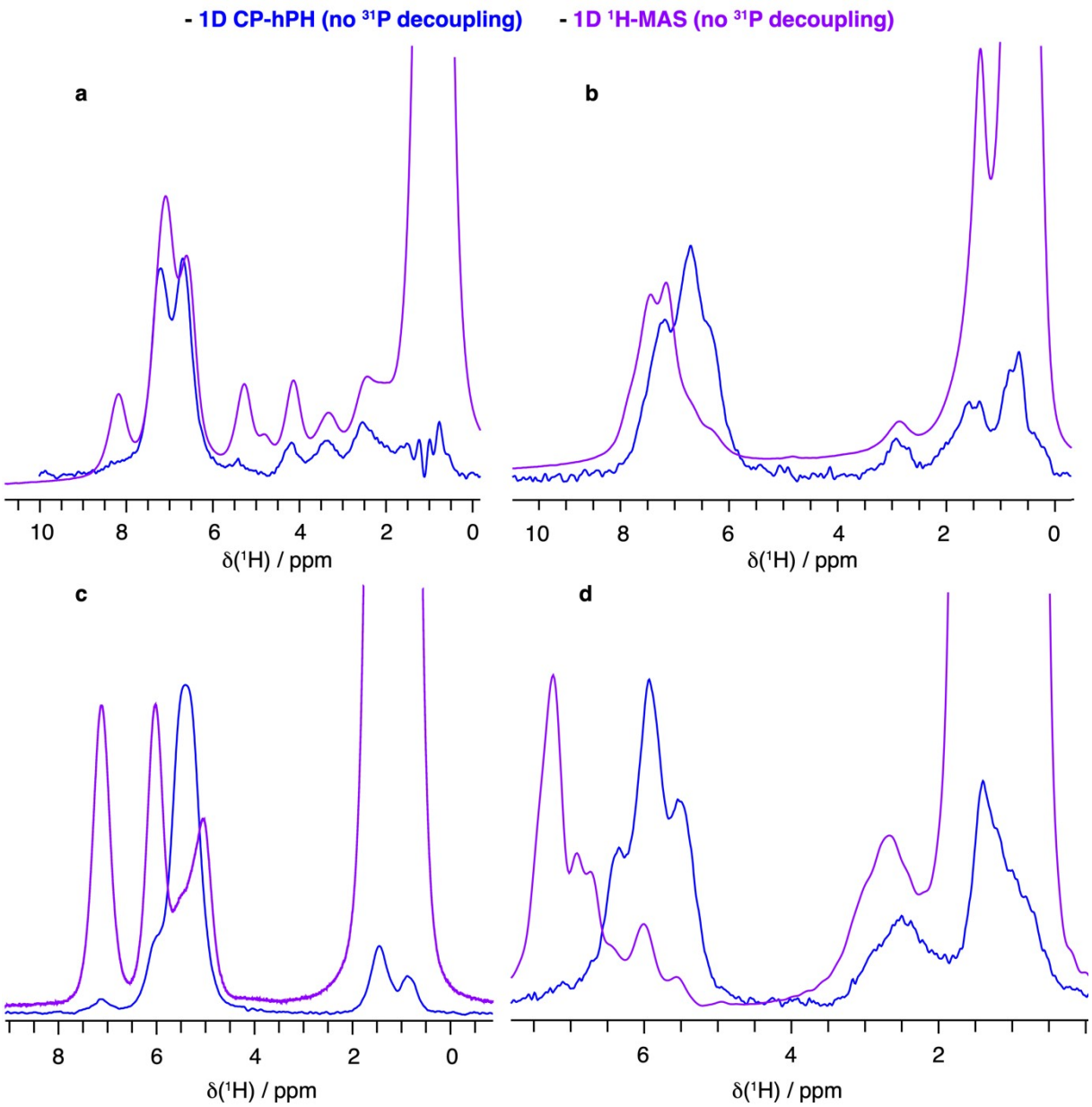

Figure S9: *hPH filtering is essential for resolving overlap issues and precisely probing ^{31}P-^{1}H connectivities.* Comparison of ^{1}H-MAS spectra (violet) with one-dimensional CP-hPH spectra (blue) without ^{31}P-decoupling during acquisition for compounds **1(a), 2(b), 3(c), 4(d)** at 100 kHz MAS and 20.0 T.

Table S2: Experimental solid-state NMR parameters.

1D ^{1}H with/without ^{31}P decoupling	**Compound 1**	**Compound 2**	**Compound 3**	**Compound 4**
ν_r/ kHz	100	100	100	100
B_0/ T	20.0	20.0	20.0	20.0
$\nu_1(^1H)$ / kHz	150	150	150	150
$\nu_{dec}(^{31}P)$ / kHz	Off/5	Off/5	Off/5	Off/-
t increments	8192	8192	8192	131072
Sweep width (t_2)/ ppm	46.7	46.7	46.7	588
Acquisition time (t_2)/ ms	103	103	103	762
Interscan delay/ s	5	2	2	2
Number of scans	32	32	32	128
Measurement time/ min	2.6	1.1	1.1	4.3

Table S3: Experimental solid-state NMR parameters (continued).

2D ^{1}H-^{1}H SD	**Compound 1**	**Compound 2**	**Compound 3**	**Compound 4**
ν_r/ kHz	100	100	100	100
B_0/ T	20.0	20.0	20.0	20.0
Transfer I	Spin Diffusion	Spin Diffusion	Spin Diffusion	Spin Diffusion
$\nu_1(^1H)$/ kHz	150	150	150	150
SD Mixing Time / ms	50	50	50	50
^{1}H carrier/ ppm	3.2	3.2	3.2	3.1
t_1 increments	700	700	800	800
Sweep width (t_1)/ ppm	47	47	47	47
Acquisition time (t_1)/ ms	8.7	8.7	10	10
t_2 increments	8192	8192	8192	16384
Sweep width (t_2)/ ppm	46.7	46.7	46.7	117
Acquisition time (t_2)/ ms	103	103	103	82
Interscan delay/ s	2	2	2	2
Number of scans	16	16	16	16
Measurement time/ h	6.2	6.2	7.1	7.1

Table S4: Experimental solid-state NMR parameters (continued).

1D ^{31}P CP-MAS	**Compound 1**	**Compound 2**	**Compound 3**	**Compound 4**
ν_r/ kHz	100	100	100	100
B_0/ T	20.0	20.0	20.0	20.0
$\nu_1(^1H)$ / kHz	150	150	150	150
$\nu_{dec}(^1H)$ / kHz	10	10	10	10
Transfer I	H-P CP (DQ)	H-P CP (DQ)	H-P CP (DQ)	H-P CP (DQ)
$\nu_1(^1H)$ / kHz	70	70	71	67
$\nu_1(^{31}P)$ / kHz	20	20	25	28
Shape	Tangent ^{1}H	Tangent ^{1}H	Tangent ^{1}H	Tangent ^{1}H
t increments	8192	8192	8192	8192
Sweep width / ppm	484	484	242	404
Acquisition time *t* / ms	24.5	24.5	49.2	24.6
Interscan delay/ s	2	2	2	5
Number of scans	512	512	128	2496
Measurement time/ min	17	17	4.2	208

Table S5: Experimental solid-state NMR parameters (continued).

Natural Abundance 2D hCH	**hCH**
ν_r/ kHz	100
B_0/ T	28.2
Transfer I	HC-CP (DQ)
$\nu_1(^1H)$/ kHz	78
$\nu_1(^{13}C)$/ kHz	22
CP contact time/ ms	1
Shape	Tangent ^{1}H
Transfer II	CH-CP (DQ)
$\nu_1(^1H)$/ kHz	78
$\nu_1(^{13}C)$/ kHz	22
CP contact time/ ms	1
Shape	Tangent ^{1}H
^{1}H carrier/ ppm	4.8
^{13}C carrier/ ppm	100
t_1 increments	148
Sweep width (t_1)/ ppm	200
Acquisition time (t_1)/ ms	2.5
t_2 increments	32768
Sweep width (t_2)/ ppm	46.3
Acquisition time (t_2)/ ms	295
^{13}C decoupling power/ kHz	5
Interscan delay/ s	4
Number of scans	128
Measurement time/ h	21

Table S6: Experimental solid-state NMR parameters (continued).

2D hPH without/with ^{31}P decoupling	**Compound 1**	**Compound 2**	**Compound 3**	**Compound 4**
ν_r/ kHz	100	100	100	100
B_0/ T	20.0	20.0	20.0	20.0
Transfer I	HP-CP (DQ)	HP-CP (DQ)	HP-CP (DQ)	HP-CP (DQ)
$\nu_1(^1H)$/ kHz	72	70	71	67
$\nu_1(^{31}P)$/ kHz	18	21	25	28
CP contact time/ ms	2.0	2.0	2.0	2.5
Shape	Tangent ^{1}H	Tangent ^{1}H	Tangent ^{1}H	Tangent ^{1}H
Transfer II	PH-CP (DQ)	PH-CP (DQ)	PH-CP (DQ)	PH-CP (DQ)
$\nu_1(^1H)$/ kHz	72	70	71	67
$\nu_1(^{31}P)$/ kHz	18	21	25	28
CP contact time/ ms	2.0	2.0	2.0	2.5
Shape	Tangent ^{1}H	Tangent ^{1}H	Tangent ^{1}H	Tangent ^{1}H
^{1}H carrier/ ppm	4.8	4.8	4.8	4.8
^{31}P carrier / ppm	-4.8	-24	-69	-8.6
t_1 increments	256	256	256	256
Sweep width (t_1)/ ppm	30	30	30	30
Acquisition time (t_1)/ ms	12.4	12.4	12.4	12.4
t_2 increments	8192	8192	8192	8192
Sweep width (t_2)/ ppm	46.7	46.7	46.7	46.7
Acquisition time (t_2)/ ms	103	103	103	103
^{31}P WALTZ64 decoupling power/ kHz	Off/5	Off/5	Off/5	Off/5
Interscan delay/ s	4	2	2	5
Number of scans	16	32	32	32
Measurement time/ h	5	5	5	11

Supplementary References

1. D. Massiot, F. Fayon, M. Capron, I. King, S. Le Calvé, B. Alonso, J.-O. Durand, B. Bujoli, Z. Gan and G. Hoatson, *Magn. Reson. Chem.*, 2002, **40**, 70-76.
2. Q. Sun, C. G. Daniliuc, G. Kehr and G. Erker, *Dalton Transactions*, 2021, **50**, 3523-3528.
3. S. Hediger, B. H. Meier and R. R. Ernst, *Chem. Phys. Lett.*, 1995, **240**, 449-456.
4. S. Hediger, B. H. Meier, N. D. Kurur, G. Bodenhausen and R. R. Ernst, *Chem. Phys. Lett.*, 1994, **223**, 283-288.
5. T. Stevens, R. Fogh, W. Boucher, V. Higman, F. Eisenmenger, B. Bardiaux, B.-J. van Rossum, H. Oschkinat and E. Laue, *J. Biomol. NMR*, 2011, **51**, 437-447.
6. W. F. Vranken, W. Boucher, T. J. Stevens, R. H. Fogh, A. Pajon, M. Llinas, E. L. Ulrich, J. L. Markley, J. Ionides and E. D. Laue, *Proteins: Structure, Function, and Bioinformatics*, 2005, **59**, 687-696.
7. R. Fogh, J. Ionides, E. Ulrich, W. Boucher, W. Vranken, J. P. Linge, M. Habeck, W. Rieping, T. N. Bhat, J. Westbrook, K. Henrick, G. Gilliland, H. Berman, J. Thornton, M. Nilges, J. Markley and E. Laue, *Nat Struct Mol Biol*, 2002, **9**, 416-418.
8. T. Suga, C. Inubushi and N. Okabe, *Acta Crystallographica Section C*, 1998, **54**, 83-85.